The 2010 IEEE/RSJ International Conference on
Intelligent Robots and Systems
October 18-22, 2010, Taipei, Taiwan

Singularity-Based Mechanism with High Responsiveness

Tomoaki Mashimo, Takateru Urakubo and Takeo Kanade

***Abstract*— We propose a singularity-based mechanism (SBM) to exploit the singular configuration that improves the angular acceleration instead of constraining the movement. The tradeoff between the responsiveness and the range of motion is achieved by varying a length of linkage in the SBM. In this paper, we clarify the responsiveness of the SBM using the dynamics analysis. For the demonstration, we build an experimental SBM system with the high responsiveness, a practical range of motion, and a size comparable to a human arm. In the experiment, the effectiveness of the SBM is shown in a vertical lifting task. The characteristic of the SBM that generates a large acceleration at start is similar to the human arm moved by a muscle. The similarity between the SBM and the human arm is analyzed in terms of the static torque.**

I. Introduction

A wide range of robots including personal robots, wearable robots, and entertainment robots, require high responsiveness. The robots employ actuators and a high reduction ratio gear to obtain a high torque (high acceleration); however, the high gear ratio limits the peak angular velocity of an output link. The actuator that obtains high angular velocity with low reduction ratio gear loses the high angular acceleration. The relations between the angular acceleration and the angular velocity are illustrated in Fig. 1. The ideal mechanism realizes the high angular acceleration at the start and the high velocity during its motion.

Generally, robot arms use electromagnetic motors with harmonic drives or reduction gears [1]–[7], motors with wires [8], [9], and motors with belts [10], [11]. In these mechanisms, the range of motion can be determined regardless of the constraint of the mechanisms. A range of motion wider than 180° is preferable for multipurpose robot arms. For examaple, the DLR lightweight arms [2] and the WAM (Barrette Technologies, USA) have a range of motion more than 180°. On the other hand, a range of motion less than 180° might be enough for personal robots such as HRP-2 (Kawada, Japan) [1] or PR1 (Willow Garage, USA) [10]. These ranges of motion are 135-140° at the elbow.

A singularity is a configuration the robot arm should avoid to prevent a degeneration of degrees of freedom. However, the mechanism effectively generates a high force at low velocity at or in the neighborhood of the singular configuration. For example, in a slider-crank mechanism composed of a crankshaft, a connecting rod, and a slider, when the crankshaft and connecting rod form a straight line, the configuration is singular. As the crankshaft and the connecting rod are straightened, the linear velocity of the slider decreases toward zero, and the thrust force of the slider increases toward infinite. The characteristic of the singularity is used for several products such as crimp tools and riveters. It has been attempted for application to robotics [12]–[14], but the dynamic performance has not been analyzed. In the mechanism, using the singularity limits the range of motion to less than 180°. That is, the relation between the range of motion and the effectiveness of the singular configuration becomes a tradeoff.

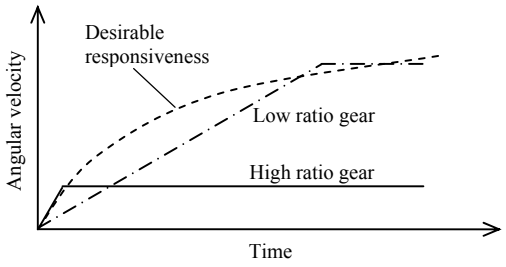

Fig. 1. The responsiveness of mechanisms. The characteristic of conventional mechanisms is determined by gear ratio and input power. The proposed singularity-based mechanism (SBM) can obtain high angular acceleration at the start and high angular velocity after acceleration.

We propose a singularity-based mechanism (SBM) that exploits the singularity and achieves high responsiveness with a practical range of motion, realizing the desirable velocity profile shown in Fig. 1. At the start, the SBM generates the high angular acceleration by high torque at low angular velocity near the singularity. After accelerating, the SBM shifts the motion with low angular acceleration at high angular velocity. In this paper, this responsiveness of the SBM is analyzed by varying the linkage lengths, which determines the range of motion. In the experiment, the dynamics model of the SBM is verified by two experimental SBM systems with the range of motion of 129° and 180°. The system with 180° is a four-bar parallel linkage, which is a common structure of robot arms.

The characteristics of the SBM generating high torque at the start is similar to a human arm with the muscle. The movement of two links in the SBM behaves as the linear actuator (slider-crank). The SBM generates high torque when the mechanism is extended. The human muscle also produces large passive tension when it is extended [15]. The torque of the SBM is compared with the human muscle's model in the statics.

Tomoaki Mashimo, and Takeo Kanade are with the Robotics Institute at Carnegie Mellon University, Pittsburgh, PA 15213 USA (corresponding author to provide phone: 412-268-1859; fax: 412-268-6436 tmashimo@cs.cmu.edu). Takateru Urakubo is with Department of Computer Science and Systems Engineering at Kobe University, Kobe, 657-8501 Japan.

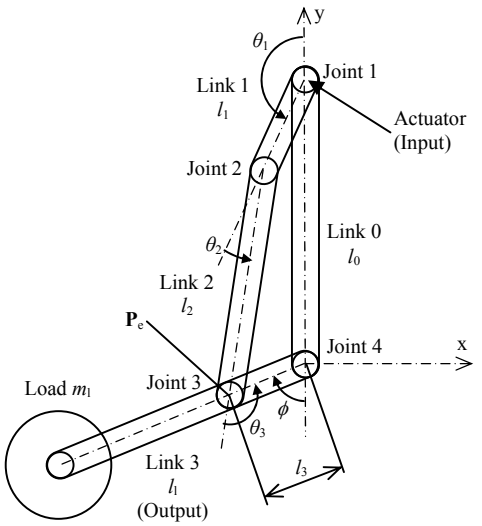

Fig. 2. Singularity-based mechanism (SBM). When the links 1 and 2 forms a straight line, the configuration is singularity.

II. Singularity-based Mechanism (SBM)

Fig. 2 shows the singularity-based mechanism (SBM), which is closed-loop four-bar linkage. The SBM is composed of links 0, 1, 2, and 3. Link 0 is fixed and the load is attached at the end of link 3. An actuator attached at joint 1 moves link 1 and the rotational direction is clockwise. When a current is applied to the actuator as an input, the motor shaft rotates link 1. Link 2 pulls link 3, and then the torque around joint 4 is obtained from link 3 as the output.

Based on the kinematic analysis of four-bar linkages [16], we derive the kinematics for the SBM. The angles of link i with respect to the link $i-1$ are denoted as θ_i for $i = 1, \cdots, 4$, and θ_1 and θ_2 are expressed in a vector form as $\mathbf{\Theta} = [\theta_1, \theta_2]^T$. An angle ϕ between link 0 and link 3 is written as $\phi = 2\pi - (\theta_1 + \theta_2 + \theta_3)$. Introducing a coordinate frame (x, y) with an origin at joint 4 and denoting a position of joint 3 as $\mathbf{p}_e = [x_e, y_e]^T$, we can express it by the following two ways:

$$\mathbf{p}_e = \begin{bmatrix} -l_3 \sin\phi \\ -l_3 \cos\phi \end{bmatrix} \triangleq \mathbf{f}_1(\phi) \ , \tag{1}$$

$$\mathbf{p}_e = \begin{bmatrix} -l_1 \sin\theta_1 - l_2 \sin(\theta_1 + \theta_2) \\ l_0 + l_1 \cos\theta_1 + l_2 \cos(\theta_1 + \theta_2) \end{bmatrix} \triangleq \mathbf{f}_2(\mathbf{\Theta}) \ , \tag{2}$$

where l_i is the length between joint i and $i+1$ and l_0 is the length between joints 1 and 4. From (1) and (2), the system has the following constraint between $\mathbf{\Theta}$ and ϕ:

$$\mathbf{\Psi}(\mathbf{\Theta}, \phi) = \mathbf{f}_2(\mathbf{\Theta}) - \mathbf{f}_1(\phi) = 0 \ . \tag{3}$$

From (2), we can obtain the following equation:

$$\dot{\mathbf{p}}_e = \mathbf{J}\dot{\mathbf{\Theta}} \ , \tag{4}$$

where $\mathbf{J}$ is the Jacobian matrix of $\mathbf{f}_2$ and can be written as

$$\mathbf{J} = \begin{bmatrix} -l_1 \cos\theta_1 - l_2 \cos(\theta_1 + \theta_2) & -l_2 \cos(\theta_1 + \theta_2) \\ -l_1 \sin\theta_1 - l_2 \sin(\theta_1 + \theta_2) & -l_2 \sin(\theta_1 + \theta_2) \end{bmatrix} . \tag{5}$$

When $\theta_2 = 0$ (links 1 and 2 form a straight line), rank of $\mathbf{J}$ is one from the above equation; that is, the configuration of the SBM including links 1 and 2 is singular. Also, when $\theta_2 = 0$, $\dot{\mathbf{p}}_e$ cannot be even in the column space of $\mathbf{J}$ from (1) and (3). Therefore, the configuration where $\theta_2 = 0$ is the singular one of the four-bar linkage mechanism, and we can obtain that $\dot{\mathbf{p}}_e = 0$ when $\theta_2 = 0$. A higher order time derivative of $\mathbf{p}_e$ can be calculated from (2) as follows:

$$\ddot{\mathbf{p}}_e = \mathbf{J}\ddot{\mathbf{\Theta}} + \dot{\mathbf{J}}\dot{\mathbf{\Theta}} \ , \tag{6}$$

$$\mathbf{p}_e^{(3)} = \mathbf{J}\mathbf{\Theta}^{(3)} + \mathbf{R}_1(\mathbf{\Theta}, \dot{\mathbf{\Theta}}, \ddot{\mathbf{\Theta}})\dot{\mathbf{\Theta}} \ , \tag{7}$$

$$\begin{aligned} \mathbf{p}_e^{(4)} = \ & \mathbf{J}\mathbf{\Theta}^{(4)} + 3\left(\frac{\partial \mathbf{J}}{\partial \theta_1}\ddot{\theta}_1 + \frac{\partial \mathbf{J}}{\partial \theta_2}\ddot{\theta}_2\right)\ddot{\mathbf{\Theta}} \\ & + \mathbf{R}_2(\mathbf{\Theta}, \dot{\mathbf{\Theta}}, \ddot{\mathbf{\Theta}}, \mathbf{\Theta}^{(3)})\dot{\mathbf{\Theta}} \ , \end{aligned} \tag{8}$$

where $\mathbf{R}_1$ and $\mathbf{R}_2$ are 2×2 matrices, and the description $(*)^{(i)}$ denotes ith order time derivative of $(*)$.

We suppose that the singular-based arm is at rest and its configuration is singular at initial time $t = 0$. A constant torque τ is supposed to be applied at joint 1 for $t \geq 0$. Since $\dot{\mathbf{\Theta}} = 0$ at the initial time, we can obtain from (1), (6) and (7) that

$$\dot{\mathbf{p}}_e = \ddot{\mathbf{p}}_e = \mathbf{p}_e^{(3)} = 0 \quad \text{at } t = 0 \ .$$

However, $\mathbf{p}_e^{(4)} \neq 0$ at $t = 0$ from (1) and (8), because $\ddot{\theta}_1$ and $\ddot{\theta}_2$ are generated by the torque τ and the column space of $\partial\mathbf{J}/\partial\theta_i$ is linearly independent from the one of $\mathbf{J}$. These results mean that the angle ϕ satisfies

$$\dot{\phi} = \ddot{\phi} = \phi^{(3)} = 0 \ , \ \phi^{(4)} \neq 0 \quad \text{at } t = 0 \ . \tag{9}$$

From (9), the time history of ϕ would be expressed by a quartic function of time near $t = 0$. The above singularity of the SBM can also be explained in terms of the relationship between small displacements of $\mathbf{\Theta}$ and $\mathbf{p}_e$ as follows:

$$\delta\mathbf{p}_e = \mathbf{O}(\delta\mathbf{\Theta}^2) \ , \tag{10}$$

where $\delta\mathbf{\Theta}$ and $\delta\mathbf{p}_e$ are small displacements of $\mathbf{\Theta}$ and $\mathbf{p}_e$ from the singular configuration respectively.

The above properties of the SBM at the singular configuration make it difficult to achieve an accurate trajectory tracking of ϕ, but they would be useful from the view of work done by the torque τ. Since $\delta\mathbf{\Theta} = \mathbf{O}(\delta\mathbf{p}_e^{\frac{1}{2}})$ from (10), the work done by τ that is represented as $\tau\delta\mathbf{\Theta}$ is relatively larger for a small displacement $\delta\mathbf{p}_e$. The work can be calculated as a function of time approximately near the singular configuration based on the dynamics of the two-link robot arm [17]. The displacement $\delta\mathbf{\Theta}$ is independent from the mass of link 3 and the weight attached to link 3, and τ can supply the energy to the system most efficiently at the singular configuration as long as the weight m_l is sufficiently heavy.

TABLE I

PARAMETERS FOR THE DYNAMIC ANALYSIS.

Quantity		Value
Length of link 0	l_0	0.3 m
Length of link 1	l_1	0.05 m
Mass of link 1	m_1	0.278 kg
Moment of inertia* of link 1	J_1	1.77×10^{-4} kgm^2
Length between joints 3 and 4	l_3	0.05 m
Length between joint 3 and weight	l_l	0.35 m
Mass of link 3	m_3	0.517 kg
Moment of inertia* of link 3	J_3	6.19×10^{-3} kgm^2
Mass of motor shaft	m_m	0.0777 kg
Moment of inertia* of motor shaft	J_m	1.38×10^{-6} kgm^2

*) Momemt of inertia about the center of gravity of each linkage.

III. RELATION BETWEEN RESPONSIVENESS AND RANGE OF MOTION IN THE SBM

A. Design of the SBM system

In this section, we analyze the relation between the responsivenss and the range of motion in the SBM sytem by varying the linkage length. The parameters of the SBM in the analysis are shown in Table I. In order to make the SBM design similar to a human arm, the link length l_0 and l_w are selected to roughly correspond the length of a human's upper arm and forearm.

We assume that the SBM starts the motion from the singular configuration at the initial angle $\phi = \phi_0$. The final angle is the sum of ϕ_0 and the range of motion Φ and is the angle that links 2 and 3 form a straight line (the second singular configuration). The range of motion Φ of the SBM is defined as the usable angle range from ϕ_0 to $\phi_0 + \Phi$. The relation between the initial angle ϕ_0 and the link length l_2 is given by the law of cosine. Therefore, the design of the SBM is determined by taking one from ϕ_0, l_2, or Φ as following:

$$\Phi = \pi - \phi_0 - \arccos\left(\frac{l_0^2 + (l_1 + l_2)^2 - l_3^2}{2l_0(l_1 + l_2)}\right) , \qquad (11)$$

In the analysis, we consider seven systems with initial angles ϕ_0 from 90° to 0° by 15° as shown in Table II and Fig. 3. From (11), when the initial angle ϕ_0 is small, the length l_2 is long and the range of motion Φ is wide. The mass and moment of inertia of link 2 increase in proportion to its length. When length l_2 is equalized to a length l_0 of link 0 ($\Phi = 180°$, $\phi_0 = 0°$), the mechanism becomes the parallelogram linkage and it transfers the input torque from actuator to joint 4 with a constant acceleration. We deal with the mechanism with $\Phi = 180°$ (Case 7) as the parallel-based mechanism (PBM) to distinguish it from the other SBM systems (Case 1 to 6) for the comparison study. In the PBM, the structure is a common mechanism for robot arms, and the dynamic characteristics are similar to robot arms with belt or wires.

TABLE II

PARAMETERS FOR THE CASE STUDY. THE RANGE OF MOTION Φ, INITIAL ANGLE ϕ_0, AND THE LENGTH l_2 OF LINK 2.

Case 1: Φ= 80.5°	ϕ_0= 90°	l_2= 0.25414 m
Case 2: Φ= 96.2°	ϕ_0=75°	l_2= 0.26665 m
Case 3: Φ= 112°	ϕ_0=60°	l_2= 0.27787 m
Case 4: Φ= 129°	ϕ_0=45°	l_2= 0.28721 m
Case 5: Φ= 146°	ϕ_0=30°	l_2= 0.29421m
Case 6: Φ= 163°	ϕ_0=15°	l_2= 0.29854m
Case 7: Φ= 180°	ϕ_0=0°	l_2= 0.300 m

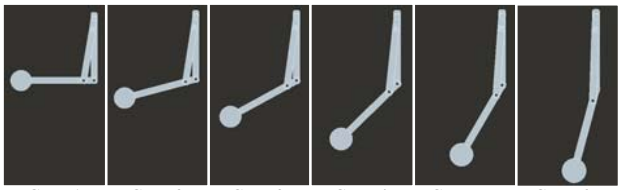

Fig. 3. Initial configuration of the SBM (Case 1 to 6). In all SBM systems, links 1 and 2 are forming a straight line ($\theta_2 = 0$).

B. Analysis Result

The motion of the SBM systems is illustrated with forward dynamics when a constant input torque τ_1 of 1 Nm is given around joint 1. In the analysis, the load m_l of 5 kg is attached at the end of link 3 and gravity is not considered to clarify the acceleration. The motion is finished at the time that the system reaches the second singular configuration.

Fig. 4(a) shows the angular displacement of seven cases. The result shows a tradeoff between the responsiveness and the range of motion. The SBM system with narrower range of motion obtains the larger angular displacement at the end time. For example, the SBM system with $\Phi = 163°$ obtains approximately 20 % higher angular displacement compared to the PBM system ($\Phi = 180°$).

The angular accelerations are shown in Fig. 4(b). At the start, the motions behave as the fourth-order function as seen in (9). The SBM systems then obtain the high angular acceleration at the start period in comparison to the PBM system. The peak of the angular acceleration of cases 1 to 6 is roughly equal. After the angular accelerations obtain the first peak, they are converged toward the constant torque of the PBM. The SBM systems again increase the angular acceleration near the second singular configuration. When the angular acceleration reaches the second singular configuration, the angular acceleration becomes zero. Thus, the high responsivenss is generated in the SBM system. The reason for zero angular acceleration is that link 1 changes to rotate in the reverse direction. The second singular configuration is both the limit of the range of motion and the point where the link 1 starts reverse rotation.

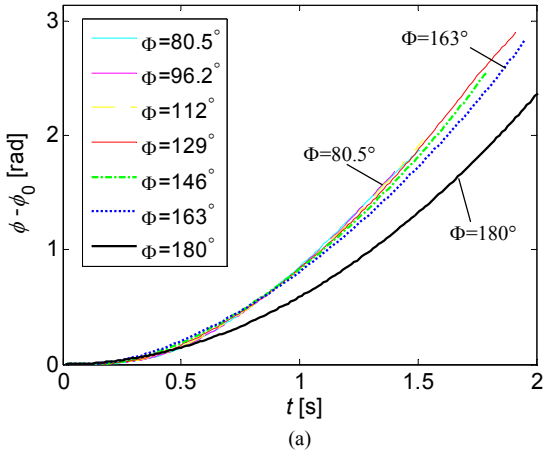

(a)

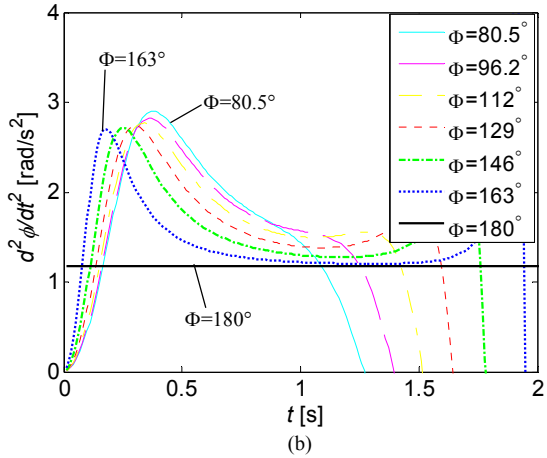

(b)

Fig. 4. Responsiveness of link 3 in the SBM. (a) Displacement and (b) angular acceleration. The high angular displacement is observed as the range of motion decreases.

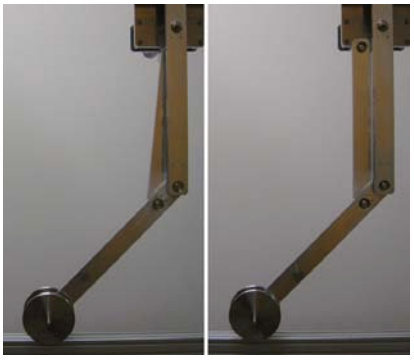

Fig. 5. Experimental setup. The SBM systems (left side) and the PBM system (right side)

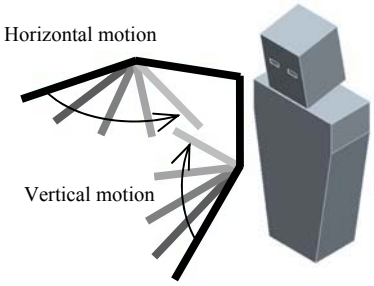

Fig. 6. Horizontal and vertical motions in the experiment. The SBM might be applied to an elbow joint of humanoid.

IV. Model Verification and Effectiveness

A. Experimental SBM System

The experimental SBM system ($\Phi = 129°$) and the PBM system ($\Phi = 180°$) are built as shown in Fig. 5. The actuator is an electromagnetic motor (EC40, Maxon Motors, Switzerland) with a planetary gear (Gear ratio: 156). A rotary encoder (HEDL5500, Avago Technologies, USA) attached to the motor shaft measures the angular displacement. Link 1 is comprised of steel for attachment to the motor shafts, and links 2 and 3 are aluminum. All joints employ bearings for a smooth rotation. The motor driver (EPOS2, Maxon Motors) provides a current to the motor and measures the actual current. A weight m_l of 1.22 kg is attached to the tip of link 3. The current is stopped when the angular displacement reaches $\phi - \phi_0 = 90°$ to prevent collision.

B. Experiment

The dynamics model is verified by the experiment and the effectiveness is demonstrated in two ways: a horizontal motion and a vertical motion, as shown in Fig. 6. The horizontal and vertical motions are determined by the installation of the experimental system. Link 0 is fixed vertically in the vertical motion. In the SBM system, the angle θ_2 is $0°$ and the angle ϕ_0 is $45°$ at the initial angle. In the PBM system, the angle θ_2 and ϕ_0 are both $45°$ and transfers a constant torque from link 1 to link 3 regardless of the angle.

In the experiment, we choose the magnitude of the input current to obtain the $90°$ angular displacement within 1 s. The current is constant to evaluate the dynamic characteristics.

1) Effectiveness in Horizontal Motion: Fig. 7 shows the time history response of the angular displacements in the horizontal motion when the constant input current of 1 A (approximately 3 Nm at the motor) is applied. The experimental result of both the SBM and PBM systems are roughly accorded to the estimated result. The delay of the angular displacement at the start is observed in the SBM system because of the start expressed as the forth-order function in (8). There is no large difference of the displacements between the two systems. The load m_l = 1.2 kg was too small to obtain the effectiveness of the singularity, compared to the analysis in the previous section (m_l = 5 kg). The SBM makes the difference larger and is effective if the load is large. (in which case, the total responsiveness is reduced.)

2) Effectiveness in Vertical Motion: The time history response of the vertical motion is shown in Fig. 8 when the constant current of 2 A (approximately 6 Nm) is applied. After 0.2 s, the difference of both systems is enlarged as time passes. Finally, the angular displacement of the SBM system

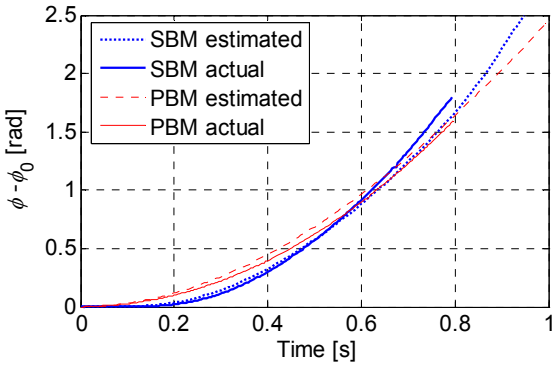

Fig. 7. Responsiveness of the SBM systems and the PBM system in the horizontal motion.

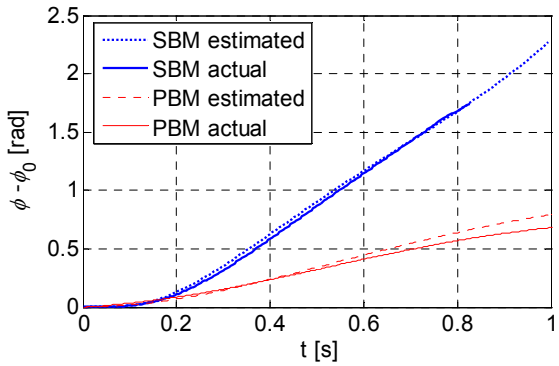

Fig. 8. Responsiveness of the SBM systems and the PBM system in the vertical motion.

is approximately two times larger than that of the PBM system. Thus, the high responsiveness of the SBM system using the singularity is obtained in the vertical motion. The reason for the effectiveness is that links 1 and 2 can store much higher kinematic energies than link 3 based on the kinematics. The SBM system can supply energy efficiently at the singular configuration when the SBM quickly lifts a load against gravity.

From the aspect of energy consumption, the SBM system supplies a large mechanical energy to the load more rapidly with the equal constant current. The back-electromotive force increases as the angular velocity increases. The SBM system has consumed higher electric energy for higher displacement than the PBM.

V. Statics Analysis of the Human Arm Model and the SBM Model

In this section, we discuss the similarity of the static characteristics of the SBM to that of a human arm. The movement of links 1 and 2 in the SBM system behaves as the slider-crank and linear actuator. The SBM can generate high torque when the mechanism is extended. The human muscle also produces a large passive tension when it is extended.

Let us build the human arm model with a muscle instead of links 1 and 2 in the SBM as shown in Fig. 9(a). Link 0 is the upper arm and link 3 is the forearm. The muscle is

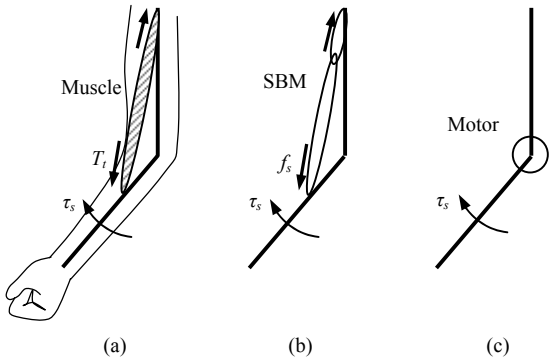

Fig. 9. Models for static analysis. (a) Human arm model, (b) SBM model, and (c) motor model.

connected from joint 1 to joint 3. Assume that the natural length of muscle is l_2, the displacement of the muscle is l_m, and the peak of the displacement is l_{mpeak}. When the peak active tension T_a and the peak passive tension T_p are given, the total tension T_t is the sum of the active and passive tensions and is expressed as [15]

$$T_t = \alpha \left(\frac{-T_a l_m^2}{l_2^2} + T_a \right) + \frac{T_p \left(e^{k l_m / l_{mpeak}} - 1 \right)}{e^k - 1} \ , \quad (12)$$

where α is a scaling variable and k is a shape parameter. In case the arm is fully stretched at the initial angle ϕ_0, the muscle is fully extended with the displacement $l_m = l_{mpeak}$. When the arm is fully flexed at the end angle $\phi_0 + \Phi$, the muscle is fully contracted with the displacement $l_m = -l_{mpeak}$. The torque τ_s generated by the tension T_t is expressed as

$$\tau_s = l_3 T_t \sin(\pi - \theta_3) \ , \quad (13)$$

where θ_3 is the angle between link 3 and the muscle. As shown in Fig. 9(b), the static force f_s of the SBM model is taken on the line connecting from joint 1 to joint 3. When the input torque τ_1 is given around joint 1, the static force f_s of joint 3 that is pulled by link 2 is expressed as

$$f_s = \frac{\tau_1}{l_1} \frac{\cos(\theta_1 + \theta_2 - \pi)}{\sin \theta_2} \quad (14)$$

In the SBM, the displacement on the line connecting joints 1 to 3 is also denoted as l_m. The SBM takes the singluar configuration at the initial angle ϕ_0 when links 1 and 2 form a straight line and $l_m = l_{mpeak}$. When the arm is fully flexed, the displacement is $l_m = -l_{mpeak}$. In order to obtain the length-tension curve of the human arm model and the SBM model, the parameters are chosen as:

$$\begin{aligned} \alpha &= 1, k = 4, T_a = 20\mathrm{N}, T_p = 40\mathrm{N}, \tau_1 = 1\mathrm{Nm} \\ \phi_0 &= 45^\circ, l_{mpeak} = 0.05\mathrm{m}, l_2 = 0.28721\mathrm{m} \end{aligned}$$

Fig. 10 shows the length-tension curve of the human arm model and the SBM. Especially, the SBM model is roughly accorded to the human arm model while the l_m is large (the arm is extened).

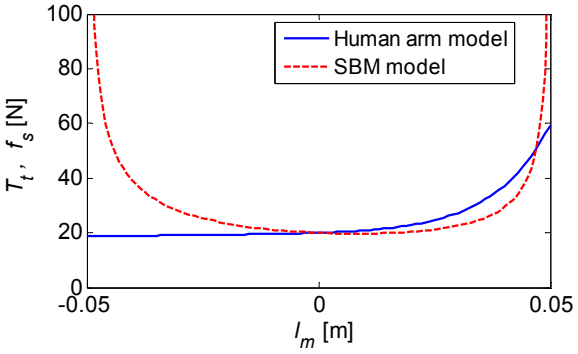

Fig. 10. Length-tension curve of the human arm model and the SBM model.

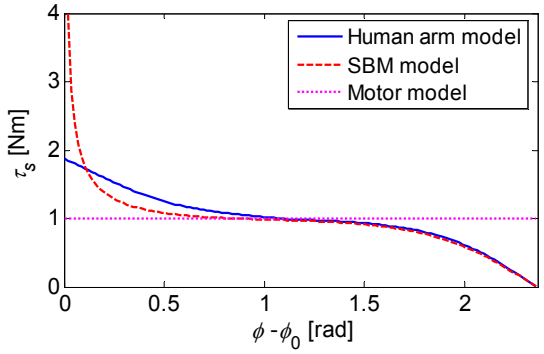

Fig. 11. Relation between the static torque and the angular displacement of the human arm model, the SBM model, and the motor model.

The static torque of the human arm model and the SBM model is derived by (13). As shown in Fig. 11, the displacement-torque curve shows a certain similarity of the human arm model and the SBM model in the statics. To compare the similarity to a torque generated by a motor, one link model with a motor (Motor model in Fig. 9(c)) is illustrated. The motor model generates the constant output torque by constant input energy. In order to obtain high torque at the start period, the motor model requires a high current and loses the input energy as heat in proportion to the amount of the current. In other words, the SBM can reduce the heat dissipation and obtain high responsiveness as well as the human arm.

VI. Conclusion

The SBM demonstrated the high responsiveness with a practical range of motion. It is especially effective in vertical motions such as a lifting task. Because of the high angular acceleration, we will obtain high dynamic torque from the system. The high torque mechanism is expected for a wide range of applications; as a mechanism for home robots, the SBM should use a spring for back-drivability and safety because the inertia of output link in the SBM becomes heavy near the singular configuration.

The SBM as a linear actuator, such as muscle, shows a certain similarity in static torque to the human arm. We estimate that the SBM is appropriate as the actuator in term of the torque for realizing an anthropomorphic arm, compared with the robot arms that employ motors at the joint. In order to confirm the similarity, the dynamics of the human arm with muscles is also a future work to be clarified. We will pursue the dynamic analysis of the singularity-based mechanism and develop applications for it's use.

References

[1] K. Nishiwaki, T. Sugihara, S. Kagami, F. Kanehiro, M. Inaba, and H. Inoue, "Design and development of research platform for perception-action integration in humanoid robot: H6," in Proc. IEEE/RSJ International Conference on Intelligent Robots and Systems, 2000, pp. 1559-1564 vol.3.

[2] G. Hirzinger, A. Albu-Schaffer, M. Hahnle, I. Schaefer, and N. Sporer, "On a new generation of torque controlled light-weight robots," in Proc. IEEE International Conference on Robotics and Automation, 2001, pp. 3356-3363 vol.4.

[3] H. Kawamoto and Y. Sankai, "Power Assist System HAL-3 for Gait Disorder Person," in Computers Helping People with Special Needs, 2002, pp. 19-29.

[4] K. Kaneko, F. Kanehiro, S. Kajita, H. Hirukawa, T. Kawasaki, M. Hirata, K. Akachi, and T. Isozumi, "Humanoid robot HRP-2," in Proc. IEEE International Conference on Robotics and Automation, 2004, pp. 1083-1090 Vol.2.

[5] T. Asfour, K. Regenstein, P. Azad, J. Schroder, A. Bierbaum, N. Vahrenkamp, and R. Dillmann, "ARMAR-III: An Integrated Humanoid Platform for Sensory-Motor Control," in Proc. IEEE-RAS International Conference on Humanoid Robots, 2006, pp. 169-175.

[6] P. Deegan, R. Grupen, A. Hanson, E. Horrell, S. Ou, E. Riseman, S. Sen, B. Thibodeau, A. Williams, and D. Xie, "Mobile manipulators for assisted living in residential settings," Autonomous Robots, vol. 24, no. 2, pp. 179-192, 2008.

[7] P. Ill-Woo, K. Jung-Yup, L. Jungho, and O. Jun-Ho, "Mechanical design of humanoid robot platform KHR-3 (KAIST Humanoid Robot 3: HUBO)," in Proc. IEEE-RAS International Conference on Humanoid Robots, 2005, pp. 321-326.

[8] K. Salisbury, W. Townsend, B. Ebrman, and D. DiPietro, "Preliminary design of a whole-arm manipulation system (WAMS)," in Proc. IEEE International Conference on Robotics and Automation, 1988, pp. 254-260 vol.1.

[9] R. Brooks, L. Aryananda, A. Edsinger, P. Fitzpatrick, C. C. Kemp, U.-M. O'Reilly, E. Torres-Jara, P. Varshavskaya, and J. Weber, "Sensing and Manipulating Built-for-human Environments," International Journal of Humanoid Robotics, vol. 1, no. 1, pp. 1-28, 2004.

[10] K. A. Wyrobek, E. H. Berger, H. F. M. Van der Loos, and J. K. Salisbury, "Towards a personal robotics development platform: Rationale and design of an intrinsically safe personal robot," in Proc. IEEE International Conference on Robotics and Automation, 2008, pp. 2165-2170.

[11] B. Driessen, H. Evers, and J. v Woerden, "MANUS-a wheelchair-mounted rehabilitation robot," Proceedings of the Institution of Mechanical Engineers, Part H: Journal of Engineering in Medicine, vol. 215, no. 3, pp. 285-290, 2001.

[12] J. Kieffer, "Differential analysis of bifurcations and isolated singularities for robots and mechanisms," IEEE Transactions on Robotics and Automation, vol. 10, no. 1, pp. 1-10, 1994.

[13] T. Takaki and T. Omata, "100g-100N finger joint with load-sensitive continuously variable transmission," in Proc. IEEE International Conference on Robotics and Automation, 2006, pp. 976-981.

[14] S. Kotosaka, and H. Otaki, "Selective Utilization of Actuator for a Humanoid Robot by Singular Configuration," Journal of the Robotics Society of Japan (In Japanese,) vol.25, no.8, pp. 115-121, 2007.

[15] N. Gialias and Y. Matsuoka, "Muscle Actuator Design for the ACT Hand," Proc. IEEE International Conference on Robotics and Automation, 2004, pp. 3380-3385.

[16] E. J. Haug, "Computer-Aided Kinematics and Dynamics of Mechanical Systems," Basic Method. Boston, MA: Allyn and Bacon, 1989.

[17] T. Urakubo, T. Mashimo, and T. Kanade, "Optimal Placement of a Two-Link Manipulator for Door Opening," in Proc. IEEE/RSJ International Conference on Intelligent Robots and Systems, 2009, pp. 1446-1451.